J Mater Sci: Mater Electron (2017) 28:17278–17282
DOI 10.1007/s10854-017-7659-y

# Excellent thermal stability and low dielectric loss of $(1-x)BaTiO_3$–$xBi(Li_{0.5}Nb_{0.5})O_3$ solid solutions in a broad temperature range applied in X8R

**Xiuli Chen[1] · Xiaoxia Li[1] · Guisheng Huang[1] · Gaofeng Liu[1] · Xiao Yan[1] · Huanfu Zhou[1]**

Received: 4 June 2017 / Accepted: 4 August 2017 / Published online: 9 August 2017


**Abstract** $(1-x)BaTiO_3$–$xBi(Li_{0.5}Nb_{0.5})O_3$ [$(1-x)$BT–$x$BLN, $0 \le x \le 0.1$] lead-free ceramics were prepared via a conventional solid state reaction method. Raman spectra and X-ray diffraction results confirmed the phase transformation from tetragonal to pseudo cubic symmetry at $0 \le x \le 0.02$. With adding $Bi(Li_{0.5}Nb_{0.5})O_3$, the thermal stability of permittivity and dielectric loss of ceramics were improved. Especially, 0.9BT–0.1BLN ceramics exhibited good dielectric properties with small $\Delta\varepsilon/\varepsilon_{25\,^\circ C}$ values ($\le \pm 15\%$) in a wide temperature range of −61–160 °C, high relative permittivity (~1500–1750) and low dielectric loss ($\tan\delta \le 0.02$) from −60 to 200 °C, which indicates that BT–BLN is candidate for X8R devices.

## 1 Introduction

Multi-layer ceramic capacitors (MLCCs) are widely used in the miniaturization of electronic components because of their excellent properties [1]. Due to high stable permittivity and low dielectric loss, perovskite materials with have been extensively researched for multilayer ceramic capacitors (MLCCs). Lead-based perovskite ceramics materials exhibited good dielectric properties, such as $Pb(Zr,Ti)O_3$, $Pb(Zr,Sn,Ti)O_3$, $Pb(Mg_{1/3}Nb_{2/3})O_3$, etc. [2–7], which could be widely applied in MLCC devices. However, PbO is toxic and volatile in high temperature, which harms to the human body and causes environmental pollution [8, 9]. Therefore, searching for environmentally friendly materials to substitute lead-based perovskite materials is extremely urgent.

$BaTiO_3$ (BT) has been extensively studied and applied to capacitor applications for many years due to its good dielectric properties [1], which makes it become the materials to replace the lead-based ceramics. Nevertheless, pure BT ceramics have three phase transitions at 125 °C (from a tetragonal phase to a cubic phase), 0 °C (from an orthorhombic to a tetragonal phase), and −90 °C (from a rhombohedral to an orthorhombic) [10], leading to the anomaly of the three dielectric, which limits their further applications in the electronic information industry. In order to enhance the thermal stabilities of $BaTiO_3$ ceramics, one of effective methods is formatting solid solutions with other perovskite compounds. Tinberg et al. reported that $BiMeO_3$ ($Me = Mg_{0.5}Ti_{0.5}$, $Ni_{0.5}Ti_{0.5}$, $Mg_{0.5}Zr_{0.5}$, etc) could form solid solutions with $BaTiO_3$, which improves the thermal stability of materials [11–14]. In our previous works, good temperature-stable dielectric behavior was obtained in $BaTiO_3$–$Bi(Li_{1/3}Zr_{2/3})O_3$ ceramics, which is extremely attractive for MLCCs of EIA (Electronic Industries Association) X7R (the change of the capacitance is ≤15% in the temperature range from −55 to 125 °C). With the application of electronic devices in harsh environment [15, 16], EIA X7R specification cannot meet the demands. Therefore, it is important to investigate and develop high-performance $BaTiO_3$-based perovskite materials with high and stable permittivity to satisfy the requirement of EIA X8R which is specified at −55 to

✉ Xiuli Chen
cxlnwpu@163.com

✉ Huanfu Zhou
zhouhuanfu@163.com

[1] Guangxi Ministry-Province Jointly-Constructed Cultivation Base for State Key Laboratory of Processing for Non-ferrous Metal and Featured Materials, Guangxi Key Laboratory in Universities of Clean Metallurgy and Comprehensive Utilization for Non-ferrous Metals Resources, Collaborative Innovation Center for Exploration of Hidden Nonferrous Metal Deposits and Development of New Materials in Guangxi, School of Materials Science and Engineering, Guilin University of Technology, Guilin 541004, China

150 °C characteristics. On the basis of previous work, we can know that Nb and Zn co-substitution for Ti at B-site can well improve the property of BT [17]. And good temperature-stable dielectric behavior was obtained in $BaTiO_3$–$Bi(Li_{1/3}Ti_{2/3})O_3$ [18]. So it could be expected that $BaTiO_3$–$Bi(Li_{0.5}Nb_{0.5})O_3$ can also display excellent dielectric performance. Therefore, $BaTiO_3$–$Bi(Li_{0.5}Nb_{0.5})O_3$ solid solution was designed and prepared by the solid state reaction method. Furthermore, the phase evolution, microstructure and dielectric properties of ceramics were also investigated.

## 2 Experimental

$(1-x)BaTiO_3$–$xBi(Li_{0.5}Nb_{0.5})O_3$ [$(1-x)$BT–$x$BLN, $0 \le x \le 0.1$] ceramic samples were prepared by the solid state reaction process using the starting materials of $BaCO_3$ (99%), $TiO_2$ (99%), $Li_2CO_3$ (98%), $Bi_2O_3$ (99%) and $Nb_2O_5$ (99%). Stoichiometric proportions of BT and BLN were weighed and milled in alcohol medium using zirconia balls for 4 h. After drying, the powders were calcined at 1100 and 650 °C for 4 h in air, respectively. Then, $(1-x)$BT–$x$BLN($0 \le x \le 0.1$) compositions were weighed and milled in alcohol medium using zirconia balls for 4 h. After drying, the powders were mixed with 5% polyvinyl alcohol (PVA) and pressed into pellets with 12 mm in diameter and 1.2 mm in thickness by uniaxial pressing at a pressure of 200 MPa. The pellets were embedded with the same calcined powders to avoid elements volatilization and sintered at different temperatures for 2 h in air (1280–1380 °C), depending on the content of BLN.

X-ray diffraction (XRD) patterns were recorded at room temperature using an X-ray diffractometer (XRD, Model X'Pert PRO; PANal ytical, Almelo, the Netherland) with CuKα radiation ($\lambda = 0.15406$ nm) operated at 40 kV and 40 mA with a step size of 0.02°. The phase analysis for the XRD data was performed by PanAlytical software (X'PertHighscore Plus). Raman spectroscopy was carried out on a Thermo Fisher Scientific DXR using a 10 mW laser with a wave length of 532 nm. The microstructural observation of the sintered samples was performed using a scanning electron microscopy (Model JSM6380-LV SEM, JEOL, Tokyo, Japan). Silver electrodes were coated on both sides of the pellets, and then fired at 650 °C for 30 min. Dielectric properties were measured with an applied voltage of 500 mV over 100 Hz–1MHz from room temperature to 400 °C using a precision impedance analyzer (Model 4294 A, Hewlett–Packard Co, Palo Alto, CA) at a heating rate of 3 °C $min^{-1}$.

## 3 Results and discussion

Figure 1a shows the X-ray diffraction patterns of $(1-x)$ $BaTiO_3$–$xBi(Li_{0.5}Nb_{0.5})O_3$ ceramics sintered at their optimized temperatures. All the samples exhibited a pure perovskite structure without any trace of impurity phase, suggesting that BLN has diffused into the BT lattices to form a homogenous perovskite solid solution with $Bi^{3+}$ entering the $Ba^{2+}$ sites and $(Li_{0.5}Nb_{0.5})^{3+}$ occupying the $Ti^{4+}$ sites. Figure 1b illustrates the enlarged XRD pattern of angles ranging from 44° to 46° for $(1-x)$ $BaTiO_3$–$xBi(Li_{0.5}Nb_{0.5})O_3$ ceramics. With increasing $x$ values from 0 to 0.02, the (002) and (200) peaks merged into a single (200) peak, showing a transformation from tetragonal phase to pseudocubic symmetry. The (022) peak near 45° tends distinctly toward lower diffraction angles with further increasing the $x$ values, indicating the enlargement of lattices. In $BaTiO_3$–$Bi(Li_{0.5}Nb_{0.5})O_3$ system, the $Bi^{3+}$(1.03 Å ≤ r ≤ 1.61 Å) is little smaller than $Ba^{2+}$(1.35 Å in 12-fold coordination) in the A-site [19, 20], but the radius of $Li^+$ (0.76 Å) and $Nb^{5+}$ (0.64 Å) are considerably larger than $Ti^{4+}$ (0.605 Å in sixfold coordination) in the B-site [21], indicating that the substitution of B-site was the main factor to cause the increase of the lattice parameters.

Figure 2 denmonstrates the room temperature Raman spectra of $(1-x)$BT–$x$BLN ceramics. Raman spectroscopy has high sensitivity to the molecular vibrations and nonuniform distortions of the crystal lattice, therefore it is a useful technique to analyze the structural and compositional evolution of ceramics. When $0 \le x \le 0.02$, the main spectral features of ceramics contained asymmetrically broad peaks at 184, 268, 304, 712 $cm^{-1}$ and symmetrically sharp peak at 515 $cm^{-1}$, which correspond to the $BaTiO_3$ tetragonal

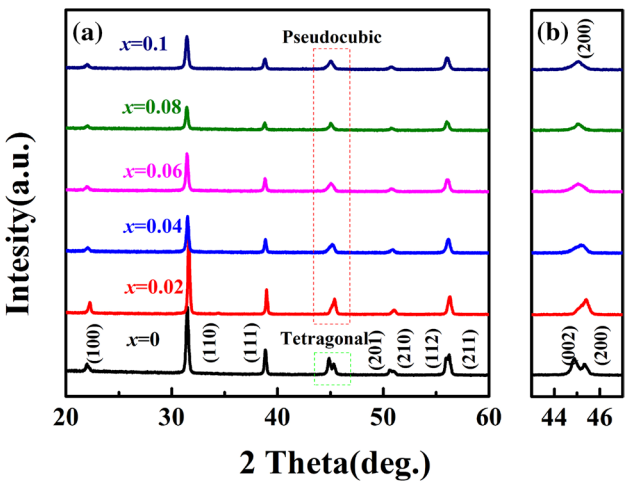


**Fig. 1** **a** X-ray diffraction patterns of $(1-x)$BT–$x$BLN ($0 \le x \le 0.1$) ceramics, **b** the enlarged XRD patterns of ceramics in the range of 2θ from 43° to 47°

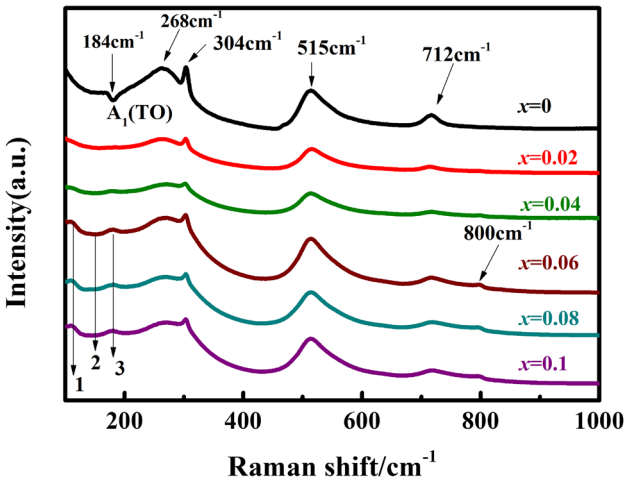


**Fig. 2** Room temperature Raman spectra of $(1-x)$BT–$x$BLN $(0 \le x \le 0.1)$ ceramics

phase [22]. The peaks at 515 and 717 $cm^{-1}$ are attributed to phonon vibrations of the Ba–O bonds, while the peaks at 184 and 268 $cm^{-1}$ are assigned with phonon vibrations of Ti–O bonds in $BaTiO_3$. The peak at 184 $cm^{-1}$ vanishes and a new mode 3 can be observed in its place, demonstrating that the long-range ferroelectric order is destroyed. With increasing $x$ values from 0.02 to 0.1, the long-range ferroelectric ordered features disappeared in the pseudo cubic symmetry, which is consistent with the XRD pattern analysis. Model 1 and Model 3 are related to the vibrations of A–O, while indicating the presence of $Ba^{2+}$ or $Bi^{3+}$ nano-sized regions [23]. At low frequencies a model 2 ppears. It may be due to the different sizes of octahedral interactions in the lattice. Besides, an octahedral breathing mode is observed at 800 $cm^{-1}$, which is Raman active for complex perovskites and solid solutions with two or more B-site species since the presence of dissimilar ions in the center of the octahedral creates asymmetry in the breathing-like mode [24].

Figure 3 illustrates the SEM micrographs of the $(1-x)$ BT–$x$BLN ceramics sintered at optimized temperatures. When $x=0$, the sample exhibited a dense microstructure with big grains. As $x=0.02$, the grain size become smaller. However, the grain size gradually increased with further increasing $x$ values. It may be $Li^+$ and $Nb^{5+}$ ions replace $Ti^{4+}$ and enter into the perovskite lattice, and the imbalance of ion valence will generate oxygen vacancies, leading to the transfer mass and energy boost, which induces the increase of the sintering behavior and grain size [25, 26].

The temperature dependences of the relative permittivity and dielectric loss of $(1-x)$BT–$x$BLN Electron$(0 \le x \le 0.1)$ ceramics in the measured temperature range from −60 to 200 °C are shown in Fig. 4. It can be seen that pure BT ceramic shows a quite sharp ferroelectric–paraelectric phase transition (Curie) peak, typical of a normal ferroelectric below Curie point ($T_c \sim 130$ °C), which agrees well with the previous reports. With increasing $x$ values, the peak values of $\varepsilon_r$ decreased from ~5500 ($x=0.02$,10 kHz) to ~1730 ($x=0.1$, 10 kHz), and broadening of the dielectric peak was observed. Similar results were also reported by Dong et al. and Yu et al. [27, 28]. With further increasing the $x$ values, the the broadening of tetragonal–cubic transition peaks disappeared above 130 °C.

Figure 5 shows the $\Delta\varepsilon/\varepsilon_{25\,^\circ C}$ and dielectric loss of $(1-x)$ BT–$x$BLN $(0.02 \le x \le 0.1)$ ceramics from −60 to 200 °C at 10 kHz. With increasing the $x$ values, the $\Delta\varepsilon/\varepsilon_{25\,^\circ C}$ and

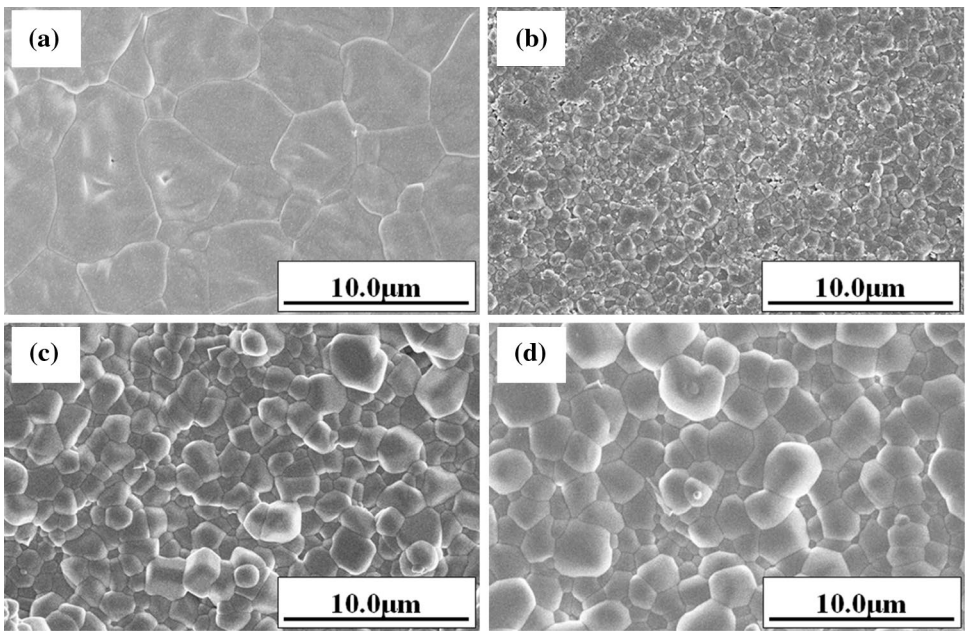


**Fig. 3** SEM micrographs of $(1-x)$BT–$x$BLN ceramic at their optimized sintered temperatures: **a** $x=0$, 1380 °C, **b** $x=0.02$, 1360 °C, **c** $x=0.06$, 1320 °C, **d** $x=0.1$, 1280 °C

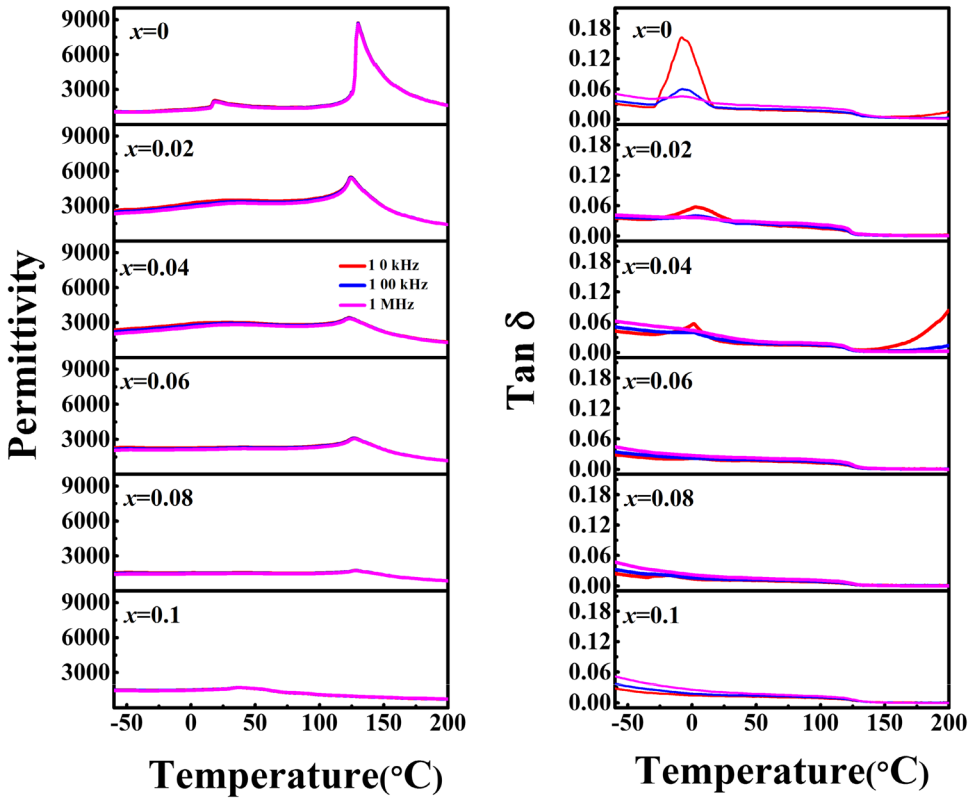


**Fig. 4** Temperature dependence of relative permittivity and dielectric loss of $(1-x)$BT–$x$BLN $(0 \le x \le 0.1)$ ceramics measured at 10 kHz, 100 kHz and 1 MHz

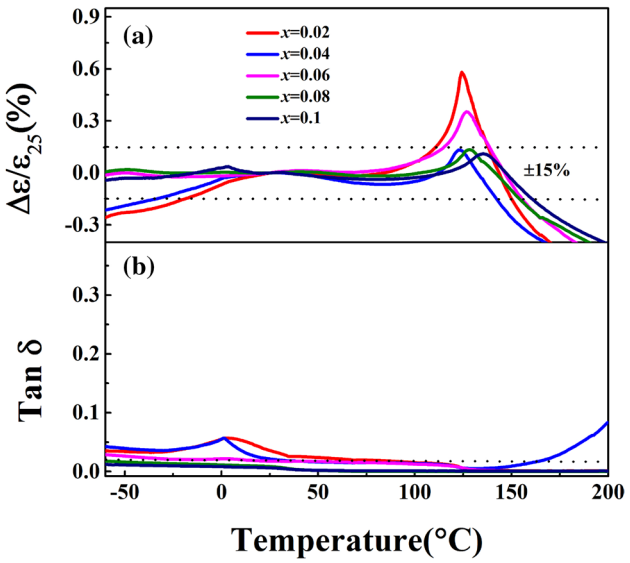


**Fig. 5** $\Delta\varepsilon/\varepsilon_{25\ ^\circ C}$ (**a**) and dielectric loss (**b**) of $(1-x)$BT–$x$BLN $(0.02 \le x \le 0.1)$ ceramics at 10 kHz

dielectric loss of ceramics were optimized. When $x = 0.1$, the excellent properties with small $\Delta\varepsilon/\varepsilon_{25\ ^\circ C}$ values (±15%) and low dielectric loss (tan $\delta \le 0.02$) from −60 to 200 °C were obtained in the temperature range of −60 to 160 °C.

The $\Delta\varepsilon/\varepsilon_{25\ ^\circ C}$, temperature dependence of relative permittivity and dielectric loss of 0.9BT–0.1BLN ceramics at 1, 10 kHz from −60 to 200 °C are demonstrated in Fig. 6. The tan δ of ceramics differed significantly in the frequency range from 10 kHz to 1 MHz, confirming the dependence of tan δ on the frequency and $x$ value. In a word, when $x = 0.1$, the ceramics exhibited the optimized dielectric properties with small $\Delta\varepsilon/\varepsilon_{25\ ^\circ C}$ values (±15%) in a wide temperature range of −60 to 160 °C, high relative permittivity (~1500–1750) and low dielectric loss (tan $\delta \le 0.02$) from −60 to 200 °C, which shown that BLN addition could significantly improve the dielectric properties of ceramics, indicating that BT–BLN ceramics are candidates for X8R applications.

## 4 Conclusions

$(1-x)$BT–$x$BLN $(0 \le x \le 0.1)$ lead-free ceramics have been investigated using the conventional solid-state processing techniques. XRD shown that BLN has diffused into the BT and form a solid solution with a single phase perovskite structure. The systematically structural transformation from tetragonal to pseudo cubic phase occurred at $0 \le x \le 0.02$. With increasing the $x$ values, an obvious decrease in the peak $\varepsilon_m$ values together with the broadening of tetragonal–cubic transition peaks were observed. When $x = 0.1$, the sample exhibited good dielectric properties with small $\Delta\varepsilon/\varepsilon_{25\ ^\circ C}$ values (±15%) in a wide temperature range of −60

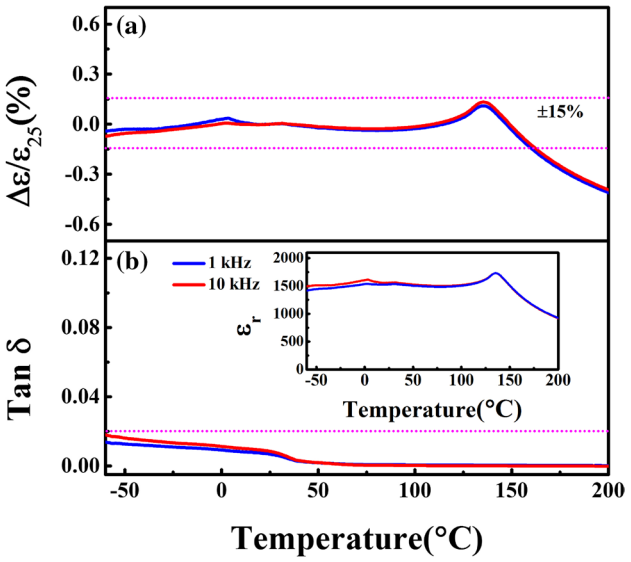


**Fig. 6** $\Delta\varepsilon/\varepsilon_{25\ ^\circ C}$ (**a**) and dielectric loss (**b**) of $(1-x)$BT–$x$BLN ($x=0.1$) ceramics at 1, 10 kHz from −60 to 200 °C. *Inset* shows the temperature dependence of relative permittivity in the temperature from −60 to 200 °C

to 160 °C, high relative permittivity (~1500–1750) and low dielectric loss (tan $\delta \leq 0.02$) from −60 to 200 °C, showing that BT–BLN is a candidate in X8R devices.

**Acknowledgements** This work was supported by Natural Science Foundation of China (Nos. 11664008, 11364012 and 11464009), Natural Science Foundation of Guangxi (Nos. 2015GXNSFDA139033 and 2014GXNSFAA118326), Research Start-up Funds Doctor of Guilin University of Technology (Nos. 002401003281 and 002401003282), and Project of Outstanding Young Teachers' Training in Higher Education Institutions of Guangxi.

## References

1. P. Ctibor, H. Seiner, J. Sedlacek, Z. Pala, P. Vanek, Ceram. Int. **39**, 5039–5048 (2013)
2. J. Chen, H.M. Chan, M.P. Harmer, J. Am. Ceram. Soc. **72**, 593–598 (1989)
3. G.H. Haertling, J. Am. Ceram. Soc. **82**, 797–818 (1999)
4. B.A. Tuttle, D.A. Payne, Ferroelectrics **37**, 603–606 (1981)
5. S. Wongsaenmai, S. Ananta, R. Yimnirun, J. Alloys Compd. **474**, 241–245 (2009)
6. L.H. Luo, H.B. Chen, Y.J. Zhu, W.P. Li, H.S. Luo, Y.P. Zhang, J. Alloys Compd. **509**, 8149–8152 (2011)
7. J.Y. Xu, M. Jin, J. Tong, M.L. Shi, X.J. Wu, B.L. Lu, L.Q. Luo, J. Alloys Compd. **449**, 36–39 (2008)
8. Y. Yuan, S. Zhang, C. Li, J. Mater. Sci. Mater. Electron. **15**, 601–606 (2004)
9. E. Aksel, J.L. Jones, Sensors **10**, 1935–1954 (2010)
10. D.H. Park, Y.G. Jung, U. Paik, J. Mater. Sci. Mater. Electron. **15**, 253–259 (2004)
11. T. Leist, J. Chen, W. Jo, E. Aulbach, J. Suffner, J. Rödel, J. Am. Ceram. Soc. **95**, 711–715 (2012)
12. S.M. Choi, C.J. Stringer, T.R. Shrout, C.A. Randall, J. Appl. Phys. **98**, 5999 (2005)
13. P. Pasierb, S. Komornicki, M. Radecka, J. Mater. Sci. Mater. Electron. **324**, 134–140 (1998)
14. A. Zeb, S.J. Milne, J. Eur. Ceram. Soc **34**, 3159–3166 (2014)
15. J.G. Kim, W.P. Tai, Y.J. Kwon, K.J. Lee, W.S. Cho, N.H. Cho, C.M. Whang, Y.C. Yoo, J. Mater. Sci. Mater. Electron. **15**, 807–811 (2004)
16. J.B. Lim, S. Zhang, N. Kim, T.R. Shrout, J. Am. Ceram. Soc. **92**, 679–682 (2009)
17. Y.L. Wang, X.L. Chen, H.F. Zhou, L. Fang, L.J. Liu, H. Zhang, J. Alloys Compd. **551**, 365–369 (2013)
18. C. Ma, X. Tan, J. Appl. Phys. **107**, 241 (2010)
19. C.C. Huang, D.P. Cann, X. Tan, N. Vittayakorn, J. Appl. Phys. **102**, 136 (2007)
20. R.D. Shannon, Acta Crystallogr. A **32**, 751–767 (1976)
21. C.B. Long, H.Q. Fan, M.M. Li, G.Z. Dong, Q. Li, Scr. Mater. **75**, 70–73 (2014)
22. A. Scalabrin, A.S. Chaves, D.S. Shim, Phys. Status Solid. **79**, 731–742 (1977)
23. J. Kreisel, P. Bouvier, M. Maglione, B. Dkhil, A. Simon, Phys. Rev. B **69**, 092104 (2004)
24. H. Yu, Z.G. Ye, J. Appl. Phys. **103**, 034114 (2008)
25. X.L. Chen, J. Chen, D.D. Ma, L. Fang, H.F. Zhou, J. Am. Ceram. Soc. **98**, 804–810 (2014)
26. M.K. Zhu, L.Y. Liu, Y.D. Hou, H. Wang, H. Yan, J. Am. Ceram. Soc. **90**, 120–124 (2007)
27. L. Dong, D.S. Stone, R.S. Lakes, J. Appl. Phys. **111**, 084107 (2012)
28. Z. Yu, C. Ang, R. Guo, A. Bhalla, Mater. Lett. **61**, 326–329 (2007)